Assessment of a Functional Electromagnetic Compatibility Analysis of Near-Body Medical Devices Subject to Electromagnetic Field Perturbation

Adel Razek

electronics

MDPI

Review

Assessment of a Functional Electromagnetic Compatibility Analysis of Near-Body Medical Devices Subject to Electromagnetic Field Perturbation

Adel Razek

Group of Electrical Engineering—Paris (GeePs), CNRS, University of Paris-Saclay and Sorbonne University, F91190 Gif-sur-Yvette, France; adel.razek@centralesupelec.fr

Abstract: This article aims to assess, discuss and analyze the disturbances caused by electromagnetic field (EMF) noise of medical devices used near living tissues, as well as the corresponding functional control via the electromagnetic compatibility (EMC) of these devices. These are minimally invasive and non-ionizing devices allowing various healthcare actions involving monitoring, assistance, diagnoses and image-guided medical interventions. Following an introduction of the main items of the paper, the different imaging methodologies are conferred, accounting for their nature, functioning, employment condition and patient comfort and safety. Then the magnetic resonance imaging (MRI) components and their fields, the consequential MRI-compatibility concept and possible image artifacts are detailed and analyzed. Next, the MRI-assisted robotic treatments, the possible robotic external matter introductions in the MRI scaffold, the features of MRI-compatible materials and the conformity control of such compatibility are analyzed and conferred. Afterward, the embedded, wearable and detachable medical devices, their EMF perturbation control and their necessary protection via shielding technologies are presented and analyzed. Then, the EMC control procedure, the EMF governing equations and the body numerical virtual models are conferred and reviewed. A qualitative methodology, case study and simple example illustrating the mentioned methodology are presented. The last section of the paper discusses potential details and expansions of the different notions conferred in the paper, in the perspective of monitoring the disturbances due to EMF noise of medical devices working near living tissues. This contribution highlights the possibility of the proper functioning of medical instruments working close to the patient's body tissues and their protection by monitoring possible disturbances. Thanks to these commitments, various health recommendations have been taken into account. This concerns piezoelectric actuated robotics, assisted with MRI and the possible use of conductive materials in this imager under certain conditions. The safe use of onboard devices with EMF-insensitive or intelligently shielded materials with short exposure intervals is also of concern. Additionally, the need to monitor body temperature in case of prolonged exposure of onboard devices to EMF is analyzed in the Discussion section. Moreover, the use of virtual tissue models in EMC testing to achieve more realistic evaluation capabilities also features in the Discussion section.

Keywords: EMF noise perturbation; functional control; EMC analysis; devices working close to tissues; monitoring; assistance; diagnosis; image-guided interventions; onboard devices

Citation: Razek, A. Assessment of a Functional Electromagnetic Compatibility Analysis of Near-Body Medical Devices Subject to Electromagnetic Field Perturbation. *Electronics* **2023**, *12*, 4780. https://doi.org/10.3390/electronics12234780

Academic Editor: Giulio Antonini

Received: 24 October 2023
Revised: 20 November 2023
Accepted: 24 November 2023
Published: 25 November 2023

1. Introduction

Electromagnetic fields (EMFs) are used in many everyday pieces of equipment. They reflect wide ranges of strength and frequency. The environment close to the EMF source devices is subject to their exposure. Unwanted exposure to such fields can cause different types of disturbances and disorders in various areas. One of the greatest areas of concern is health safety. In this case, the disorder could directly involve body tissues or healthcare diagnostic, detection and intervention devices. Regarding EMF exposure, most of the affected source devices are characterized by significant stray fields, e.g., wireless devices. The

EMF exposure of living tissues can cause different biological effects [1–6]. The other effect of EMF exposure on health safety is related to medical devices. Such exposure can disrupt several types of health devices. The devices most affected by health problems are those working near body tissues. Two important categories of devices are of concern. The first concerns imaging diagnostic procedures and image-assisted robotic interventions [7–13]. In such a case, disturbances due to EMF noise mainly concern universal non-ionizing procedures using MRI. The second category concerns body onboard embedded and wearable devices [14–18].

MRI as a diagnostic tool could be disrupted due to its sensitivity to EMF noise. This scanner is generally protected against exposure to external fields. However, EMF noise could be triggered due to the introduction of magnetic or conductive material inside or near the scaffold. This may occur due to objects inserted in the body under testing. The consequences would be image artifacts disrupting the diagnosis [19–22]. Considering the case of MRI-assisted robotic interventions, these can be surgical or implanted treatment. These procedures mainly concern situations requiring movement or location control. Thus, the assistance of concern offers remarkable means of localization and precise displacement control, improving the result of medical treatment and allowing precise minimally invasive actions. In this case, the EMF noise disturbance could be, in addition to the body tested, due to the presence of robotic accessories and medical tools within the scaffold [23–29].

The EMF noise perturbation of onboard devices is provoked by exposure to external fields (radiation). Embedded and portable devices are often used for ongoing medical assistance or for diagnostic and monitoring purposes. The case of wearable mechanisms correspond to a passive programmed role as sensing functions, e.g., [30–32]. The wearable biosensors involved behave as non-intrusive tools allowing real-time monitoring of patients, providing sufficient data to establish their health status and can constitute a first diagnosis. Devices integrated into the body can be static passive for permanent monitoring, e.g., [17], or active stimulating or assisting tools, e.g., [18]. All of these onboard tools enable diligent, personalized and tailored healthcare. Note that most of these devices may be of concern with the disturbances caused by the patient's body inside the MRI mentioned above.

The different functional disorders of devices due to EMF noise mentioned above should be evaluated and controlled. Thus, a routine of functional control could be practiced on these devices. The functional control at large verifies the ability of a device to operate in a specific environment. Regarding EMFs, generally speaking, the increasing complexity and amplified practice of electronic tools have given rise to electromagnetic interference (EMI), which involves various signals emitted in an unsolicited manner. These can affect the operation of systems in a specific electromagnetic atmosphere, causing them to fail or reducing their performance. Indeed, EMI corresponds to the transmission of disturbing energy (noise) between two systems (source and receiver) via radiating and/or conductive tracks. Such noise can come from an artificial source (like radar or a cell phone) or a natural source (like lightning). Furthermore, the noise could be intrinsic to the system due to alterations of its physical characteristics (like the effect of the insertion of external materials). Concerning EMI, the creation of an electromagnetically compatible atmosphere in relation to the affected system (receiver) allows it to regain its intended operation. Thus, EMC can be achieved to respond to EMI threats. Therefore, due to the different types of noise mentioned, the functional EMC control can be termed as verifying the ability of a device to function properly in its electromagnetic environment without interference with itself or other systems in that environment.

Consequently, the various functional disturbances of medical devices conferred above can be evaluated and controlled with an EMC analysis, e.g., [25,27,29]. This can be achieved by experimental means (where possible) or by using numerical modeling tools. Such a numerical assessment in addition to functional control can assist in the redesign of disturbed devices, disturbing sources and introduced external materials. Additionally, a numerical EMC analysis enables shielding design with validity verification regarding sources and targets of disturbances [33].

The objective of this contribution is to analyze the disturbances due to EMF noise of medical devices working, in particular, near living tissues and to synthesize the corresponding functional EMC control of these devices. This is achieved in the context of minimally invasive and non-ionizing environments enabling various health treatments involving monitoring, assistance, diagnoses, as well as image-guided medical interventions. It aims to authenticate recommendations that fit into the patient's well-being.

Section 2 of the article presents the different imaging methodologies, taking into account their nature, their operation, their conditions of use, as well as the comfort and safety of patients. MRI components and their field characteristics will be analyzed. The resulting concept of MRI compatibility and possible image artifacts will be detailed and analyzed. Section 3 concerns MRI-assisted robotic treatments. The possible robotic introductions of external materials, the characteristics of MRI-compatible materials and the conformity check of such compatibility will be analyzed and discussed. Section 4 concerns integrated, portable and detachable medical devices. In this framework, the control of EMF disturbances will be conferred and the necessary shielding protection technologies will be presented and analyzed. In Section 5, the EMC control procedure will be analyzed and discussed. The equations governing EMF and their application in EMC control will be illustrated. Digital virtual models of the body that can be involved in the actual representation of the operating area of medical devices will be discussed and reviewed. A simple qualitative methodology case study example illustrating the mentioned methodology will conclude this section. Section 6 addresses the analysis of potential extensions of the different notions mentioned in the article, with the perspective of monitoring disturbances due to EMF noise of medical devices working close to living tissues. This concerns, among other things, the particular case of prolonged exposure of onboard devices to EMF, which can trigger, in addition to a malfunction of the device, a risk of heating of tissues directly by EMF and indirectly by power dissipation in conductive metals contained in the device. In such a case, we must control, in addition to device disturbances, body temperature. The discussion also involves and details the concepts of a virtual tissue model, smart shielding, etc.

2. Imaging Methodologies

Various imaging techniques are used in healthcare treatments. The chosen option depends on several conditions related to the concerned circumstances. Living tissue imaging involves soft tissues, bones, fluids and air gaps. The most widespread techniques use X-rays, magnetic fields, ultrasound or radioactive drugs (positron emission, gamma rays, etc.). The corresponding scanners are each relatively adapted to a specific case. Apart from magnetic and ultrasound imaging techniques, the others are subject to ionizing radiation. These tools can be used for diagnostic purposes or therapeutic assistance. In conventional diagnostic imaging, patient exposure is generally short-term, posing no risk from any scanner. On the other hand, persistent exposures such as, e.g., assisted treatments, infer and take into account the comfort and safety of the patient. In addition to a minimally invasive practice, non-ionizing conditions are required. In these circumstances, only MRI and ultrasound scanners are free from ionizing radiation [9–13]. However, each of these two scanners is subject to particular limitations. Ultrasound can only work in tissues devoid of bone and air [27,29]. MRI needs an atmosphere free from external EMF noise, which must be controlled [23–29]. From the above analysis, for image-assisted treatments, MRI seems the most adequate, conditioned on controlled external EMF noise (EMC control). Figure 1 illustrates the above analysis for imaging strategy options.

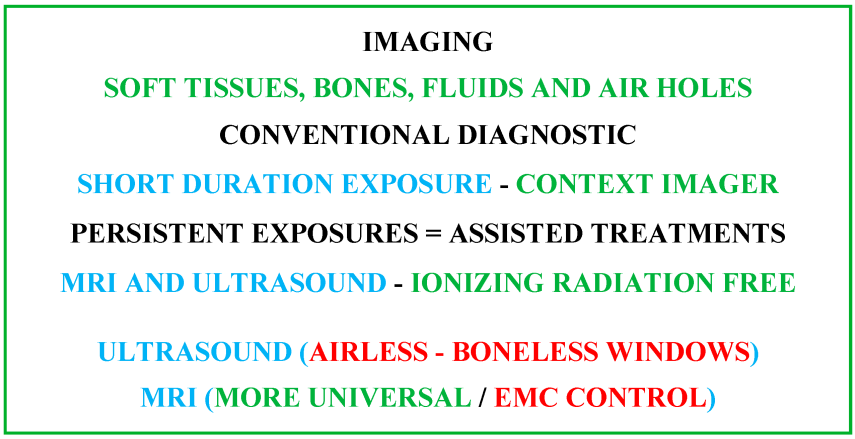

Figure 1. Summarizing diagram of imaging strategy options accounting for patient comfort and safety.

2.1. MRI Constituents

The shaped MRI image is produced using signals resulting from the interaction of biological tissues with magnetic fields. Three different feature fields are used to create 3D images. The first is a high-intensity static field. It generates a magnetizing vector in living tissue that aligns and measures the density of the protons involved. The second is linked to three low-frequency spatial gradient fields. These locate aligned tissue protons, establishing a 3D restoration of the different spatial divisions of tissue in the images. The third is a radio frequency field. This stimulates the magnetizing vector, allowing its identification with the scanner and the transformation of the effects on the tissues into images [27].

In fact, MRI theoretically aims to image the nuclei of hydrogen atoms, which are held inside living tissues. A hydrogen nucleus that is a proton is a mass of positive charge rotating on itself around an axis. In living tissue, protons are rotated randomly and do not rotate all together. As a result, they display zero subsequent magnetic field and operate out of phase. According to the principle of MRI, protons require three basic arrangements in the examined section of tissue, which align in a fixed direction all the protons, rotate them together and locate their distinct spatial origins. The aligning action could be fulfilled by the introduction of the concerned body tissue section in a high-intensity magnet to steer them simultaneously in the axial direction of its static field B_0. To reach their joint spinning, a resonance action can be applied. Thus, one can use an excitation with a radiofrequency (RF) field, B_1, having a frequency identical to that of proton rotation natural frequency f_L (Larmor frequency of protons). Localizing protons' distinct spatial positions can be achieved through the use of their related field distinctive values. Thus, a 3D space gradient, G(x, y, z), with pulsations of low-frequency repetitions can be joined to the field B_0, permitting the detection of the distinct position values of B_{0d} (x, y, z) = B_0 + G(x, y, z). The last conferred fields B_0, B_1 and G(x, y, z) reflect different natures. It is worth noting that the value of protons' Larmor frequency f_L is a function of the B_0 field value and equivalent to 42.5 MHz per tesla and hence the conforming position distinctive frequencies f_{Ld} (x, y, z) are functions of B_{0d} (x, y, z).

These three fields allow establishing images as follows. The protons are subjected to excitation–relaxation sequences by an RF energy wave, leading to energy supply restoration actions. A suitable tuned RF antenna permits the detection of the restored energy corresponding signals. These are related to the B_1 values with frequencies of f_{Ld} (x, y, z). Thus, coding of spatial imaging in the concerned tissues can be obtained. Note that B_1 frequency is f_L that is usually tuned to a value in the center of the explored tissue of f_{Ld} (x, y, z).

2.2. Features of MRI Fields B_0, G(x, y, z) and B_1

Respectively the strong magnet, gradient coils and RF coil produce these fields. In the standard procedure of MRI, its proper action necessitates the shield of the magnet and gra-

dient coils and the compensation of their fields. Indeed, a virtuous MRI requests a uniform constant B_0 (by using shimming coils) and linear uniform regulated field gradients. These fields necessitate corrections and compensations for reliable performing of the scanner.

The RF coil field seems the most exposed, and characterizes a fragility to noise fields and to near introduced external materials. The most widespread form of an RF coil is birdcage-like and is used as an exciting RF source as well as a tuned RF antenna. Figure 2 illustrates a representation of the three MRI components and their conforming fields.

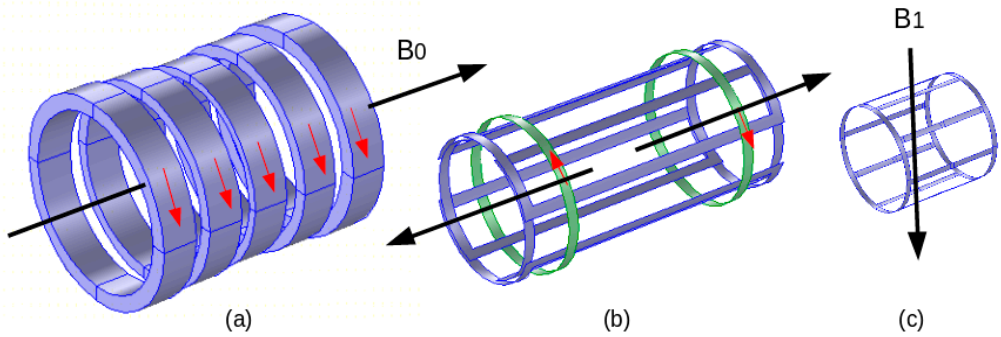

Figure 2. MRI components and corresponding fields: (**a**) electromagnet B_0, (**b**) gradient coils (one axis couple), (**c**) RF coil B_1.

The characteristics of these fields are different regarding their magnitude, pulsation and presence throughout the MRI functioning—B_0: 0.2–10 T, 0 Hz, permanently present; G(x, y, z): 0–50 mT/m, 0–10 kHz, multiple pulses of few ms; and B_1: 0–50 µT, 8–300 MHz, Amp. Mod. Pulses of few ms.

2.3. MRI Compatibility

As mentioned earlier, MRI is sensitive to EMF noise resulting from external field exposure or insertion of specific external matters (magnetic and conductor) within or close to the MRI scaffold. Conventionally, an MRI is shielded regarding external field exposure. We can largely typify an external object as MRI-compatible if it behaves in an MRI-safe manner, not affecting image quality, and working as expected. In addition, the static field magnet and the gradient coils are shielded and their fields are compensated for a reasonable size of inserted matters. As stated in the last section, only the RF coil and its field seem vulnerable for such insertion and it is necessary to control the compliance of the inserted matters with the correct functioning of the scanner. Thus, the inserted external materials should be MRI-compatible, i.e., not perturbing the RF field and image. Only non-magnetic and non-conductor matter can theoretically behave in an MRI-compatible manner. In general, magnetic materials are reduced to trivial-almost-zero sizes. Conducting materials have an indirect perturbing effect on the RF field. They exhibit eddy currents induced by the RF field that perturb the distribution of this field, which alters the image. Such induced currents are directly related to the conductor surface perpendicular to the RF field direction and hence can be reduced by minimizing such surface. Typically, a conducting sheet of negligible thickness positioned parallel to the field direction will almost not cause any field perturbation independent of its surface size. This phenomenon permits the use within the scaffold of conducting matters with specific shapes and orientations.

2.4. Image Artifacts

The image quality can be deteriorated for diverse reasons. The scanner itself can be the source of decreased image quality, as in the case of an inefficiently shimmed imager. Living tissues can also diminish the image quality due to susceptibility discrepancies, such as those between soft tissues and air holes in the brain. Moreover, embedded matters within the body such as prostheses and particularly metallic ones can also weaken image quality [34–40]. The image modification due to metallic materials, which present susceptibility

variations, depends on the size, the shape and the direction with respect to B_1 [27,29,33]. Additionally, an important cause of image artifacts could be the tools, particularly metallic ones, involved in under-imaging processing. Indeed, currents induced in metals not only mainly by the RF fields but also by low-frequency gradient fields can affect the image. These currents could interact mainly with the RF field, which is the most at risk among the fields of an MRI.

3. MRI-Assisted Robotic Treatments

As mentioned previously, in surgical or implanted treatments requiring movement or localization control with increased precision, we can use imaging-assisted robotic interventions allowing precise minimally invasive actions. Also, in such image-assisted treatments, non-ionizing MRI seems to be the most adequate, on the condition of controlled external EMF noise. Such noise can come from robotic accessories and medical tools [23–29].

3.1. Robotic External Matter Introductions

As mentioned in the last section, only non-magnetic and non-conducting materials can be used in MRI-guided robotic interventions. The robot's mainframe and therapeutic tools are normally made of non-magnetic and non-conducting materials. However, a robot needs actionable movements. Most competent actuators are the electromagnetic ones using magnetic and conductive materials. Few types of non-electromagnetic actuators with performance suitable for MRI-assisted robotic operation can be used. This could be the case for piezoelectric actuators subject to their MRI compatibility; see, e.g., [41–56]. Such actuators are made of dielectric piezoelectric materials coated with trivial electrodes. As indicated in Section 2.3, the shape and orientation of these electrodes (conductors) relative to the RF field B_1 allow possible MRI compatibility. Different keys are proposed for the mechatronic division of the robot containing electronics, sensors, actuators, etc., which address a difficult compatibility question [27,29,41–46,57–61].

3.2. MRI-Compatible Materials

Materials governed by EMF behavior can be magnetic or non-magnetic and a conductor. The non-magnetic materials can behave between dielectric and electric conducting function of EMF wave frequency. Magnetic, dielectric or conductor materials are characterized, respectively, by the permeability μ (or the susceptibility χ), by the permittivity ε or by the conductivity σ. In highly magnetic material, $\mu_r >> 1$ and $\mu_r \approx \chi$; note that $\mu = \mu_0 \cdot \mu_r$ and $\chi = \mu_r - 1$. For non-magnetic material, $\mu_r = 1$ and $\chi = 0$. The relative values of σ and $\omega \cdot \varepsilon$ ($\omega = 2\,\pi\,f$) characterize dielectric vs. electrically conducting behaviors of non-magnetic materials. For low f, $\sigma >> \omega \cdot \varepsilon \approx \sigma$ and for high f, $\omega \cdot \varepsilon >> \sigma \approx \omega \cdot \varepsilon$ and $\sigma \approx 0$.

The materials' compatibility in MRI is of two types, magnetic and electric, characterized, respectively, by μ (or χ) and σ. A fully MRI-compatible material has zero values for both χ and σ. The dielectric nature of matters does not affect the compatibility. Regarding the RF field distribution, the eventual introduced matters should have $\mu_r = 1$ and $\chi = 0$, with high $\omega \cdot \varepsilon$ (will be naturally high in RF range), or conductors with a trivial cross section (e.g., very thin sheet) perpendicular to the RF field B_1. With such features, the RF field distribution would not be altered. Note that the induced eddy currents (responsible for field perturbation) in the configured conductor by the current in the RF coil would be extremely negligible due to the trivial conductor section (see the example of Section 5.3).

3.3. Conformity Control of MRI Compatibility

The MRI-compatibility control can be accomplished for existing image-guided MRI systems by using experimental means. This can be carried out by measuring the perturbations of the field resulting in the insertion of checked objects within or near the scaffold according to the case. This is generally accomplished via sensors positioned in specific points in the system. Such techniques in the case of MRI are relatively complex due to the

necessity of special shielded expensive chambers and the self-perturbation effects of the measuring sensors. Additionally, the characteristics of a tested object could prove dangerous, leading to degradation of imager components. Furthermore, such a compatibility check is only possible for existing systems and cannot be used for the design of unbuilt systems. In these circumstances, a more advantageous solution could be a compatibility check with numerical modeling techniques via an EMC analysis for the different inserted objects [25,27,29,33]. In fact, disturbances in the distribution of EMFs in a given structure caused by the introduction of an external material are related to the EMFs produced in that material. In this case, if the EMF noise is reduced or removed, the field distribution of the target structure will be minorly or not affected.

4. Embedded, Wearable and Detachable Devices

Recent advances in the field of biocompatible and biodegradable materials [62–73] have enabled the development of implantable static passive tools enabling diagnoses and prediction via mini-sensors, thereby dramatically improving the value and efficiency of patient healthcare [74–78]. Other static but active implanted devices are proposed to stimulate or trigger an organ, as pumps, neuro-stimulators or pacemakers [79–83]. In addition, wearable devices, which behave as non-invasive tools in real-time, are available, allowing continuous monitoring of people under treatment and thus providing sufficient medical data to establish the general health status and, furthermore, a preliminary identification of the medical diagnosis [14–16,30–32]. Additionally, detachable and connectable smart sensing devices, which are also real-time health monitoring systems, exist for functional indications intimately associated with physical conditions. These indications concern the frequency of cardiac functioning, blood circulation pressure, respiratory rate, etc. Such individualized healthcare supervision provides appropriate medical information [84–86]. Figure 3 illustrates a summarized representation of the different onboard devices and their functions.

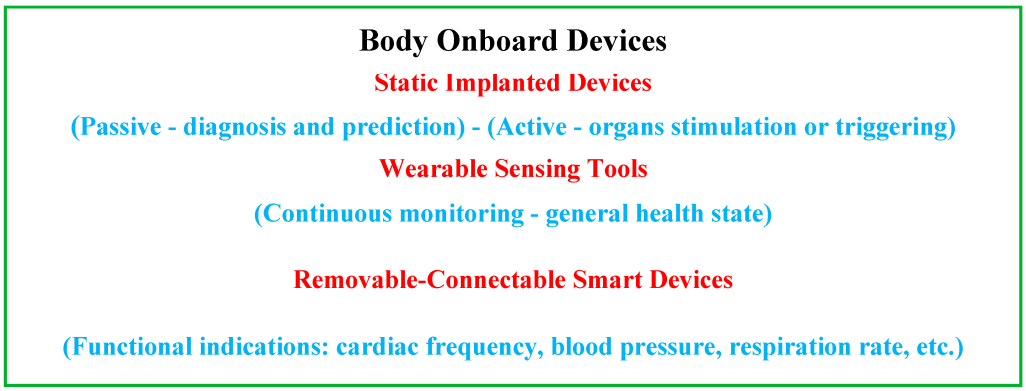

Figure 3. Summarizing diagram of the different onboard devices and their functions.

In addition to the mentioned functions, implanted devices, wearable sensing tools and removable and connectable smart devices enable healthcare providers to monitor the biological characteristics of patients after treatment [87,88]. Additionally, it should be noted that an important aspect of health administration responsibilities is increased support for integration and connection strategies for the delivery of personalized care. Therefore, it is preferable to use the paradigms of connected services and home clinics rather than face-to-face care. All three mentioned implantable, wearable and detachable strategies are involved in such individualized healthcare [89–92].

An important safety issue is the protection of devices conferred above from exposure to EMF noise emitted by nearby everyday sources. This can be accomplished in different ways. The first is to bypass EMF-sensitive materials in their makeup where possible. The second option is to protect (by shielding) these devices as well as the tools that are sources

of exposure. An additional precaution is to avoid exposing them to strong electromagnetic fields such as their insertion in the high static field of an MRI.

In the following subsections, EMC control of onboard devices as well as their protection against EMF exposure will be examined. The particular case of continuous or prolonged exposure to EMF, which needs to monitor body temperature, will be examined in Section 6 relative to the discussion.

4.1. EMF Perturbation Control of Onboard Devices

An important characteristic of an onboard device (receiver) subject to EMF exposure (source) is whether it can operate normally in an exposed atmosphere. This determines its ability to execute. However, when such a receiver device experiences EMF source emission, its main operating indicators could be disturbed by a decrease in the signal-to-noise quotient, signal delay, etc., and thus, its performance could be degraded. Depending on the area of application, a receiver device has specific usage requirements and its EMC evaluation test refers to the corresponding standards [93–95]. These are mainly based on static techniques. Therefore, the EMC evaluation test performed on the device is based on a standard framed waveform while the EMC analysis is performed and confers the test results. This difficulty of considering the dynamic behavior of a complex atmosphere of exposure to EMF is called into question by the operation of the device itself. Various works have been carried out to improve EMC evaluation testing techniques [96–101].

The test control methods described above are relatively complex and often require specific and expensive shielded spaces. Under such conditions and as in the case of Section 3.3, an alternative solution can be the control by digital calculations via an EMC analysis to verify the integrity of the various onboard devices [25,27,29,33,102]. In fact, the validity of a method protecting a device from EMF exposure could be guaranteed with an EMC check confirming that the device's fields are not changed by exposure.

4.2. Onboard Device Shielding Protection Technologies

As mentioned earlier, to reduce the effects of EMF noise exposure on implanted, portable and removable medical devices, we can use either shielding of the receiver and source or adjustment of their structures using design and optimization tools. Both strategies can be assisted and verified by the EMC analysis control.

Shielding technology generally uses materials that absorb or reflect the emitted EMF wave to prevent its passage from one side of the shielding layer to the other. EMI coatings, layers and shielding, which help retain EMF noise, are essential for the normal operation of medical devices and the protection of human health. An EMF generally consists of magnetic and electric fields directed perpendicularly in space. Therefore, EMI shielding strategies are classified into electric and magnetic EMI shields and their coupled forms. High-frequency waves such as RF EMF waves, which primarily characterize radiation, have interdependent electric and magnetic fields. Therefore, shielding one field can result in the absence of the other. Due to this phenomenon, EMI shields are generally conductive in nature. The shielding material can be of different types depending on the type of application. They are made from clothing, rubbers, adhesives and coatings. These different constitutions are correlated with the necessary flexibility, the fixing capacity, the ease of the process and the constancy. The field of EMI shielding investigation is very active due to the growth of everyday EMF noise [103–114].

5. Functional EMC Control

This section concerns the EMC control conferred in Sections 3 and 4 concerning, respectively, MRI-assisted treatments and onboard medical devices (implanted, wearable and detachable). An EMC analysis is based and governed by EMF equations, which characterize the behavior of fields. This could be the disruption of EMF distribution in a given structure by an external EMF-sensitive insertion, as in Section 3. On the other hand, it could be the disruption of EMF distribution in an EMF-sensitive target from an exposure

source, as in Section 4. In these cases, if, respectively, the inserted object or the exposed target was insensitive to EMF, the field distributions in the structure or in the target would not be affected.

5.1. EMF Governing Equations

The EMF equations derived of Maxwell theory [115] can be mathematically formulated in different frames according to the concerned problem. One of the most popular is the basic full-wave EMF formulation presented with

$$\boldsymbol{\nabla} \times \mathbf{H} = \mathbf{J} \tag{1}$$

$$\mathbf{J} = \sigma\, \mathbf{E} + \mathrm{j}\, \omega\, \mathbf{D} + \mathbf{Je} \tag{2}$$

$$\mathbf{E} = -\boldsymbol{\nabla}\, \mathrm{V} - \mathrm{j}\, \omega\, \mathbf{A} \tag{3}$$

$$\mathbf{B} = \boldsymbol{\nabla} \times \mathbf{A} \tag{4}$$

In Equations (1)–(4), **H** and **E** are the magnetic and electric fields, respectively, in $\mathrm{A{\cdot}m^{-1}}$ and $\mathrm{V{\cdot}m^{-1}}$, **B** and **D** are the magnetic and electric inductions, respectively, in T and $\mathrm{C{\cdot}m^{-2}}$ and **A** and V are the magnetic vector and electric scalar potentials, respectively, in $\mathrm{W{\cdot}m^{-1}}$ and V. **J** and **Je** are the total and source current densities in $\mathrm{A{\cdot}m^{-2}}$, σ is the electric conductivity in $\mathrm{S{\cdot}m^{-1}}$ and ω is the radial frequency pulsation equal to 2π f (f in Hz). The symbol $\boldsymbol{\nabla}$ is a vector of partial derivative operators, and its three possible implications are a gradient (product with a scalar field), divergence and curl (dot and cross products, respectively, with a vector field). The magnetic and electric comportment laws, respectively, between **B/H** and **D/E** are represented by the permeability μ and the permittivity ε, respectively, in $\mathrm{H{\cdot}m^{-1}}$ and $\mathrm{F{\cdot}m^{-1}}$.

Note that Equations (1)–(4) are a mathematical unification established by Maxwell involving an association of three experimental laws possessing physical meaning discovered by his predecessors. Maxwell–Gauss law relates the electric displacement D to the free electric charge density q, Maxwell–Ampère law links the H-magnetic field to the time-rate of the electric displacement D and the free total current density J and Maxwell–Faraday law relates the electric field E to the time-rate of the magnetic induction B. The unified Maxwell equations' set contains a key revision of Ampere's theorem.

The solution of Equations (1)–(4) allows for determining in a system the EMFs for a given frequency pulsation, taking into account the behaviors of magnetic materials via permeability, the eddy currents in electrical conductors across electrical conductivity and the displacement currents in dielectrics through permittivity. Such a solution can be achieved through local numerical discretized approaches or other methods allowing local calculations; see, e.g., [116–122].

EMF Equation Solution and EMC

An EMC analysis can monitor via such a solution EMF disturbances due to the insertion of external objects into the birdcage RF coil of an MRI (Section 3). In addition, this can control disturbances by an external EMF source in a target device, indicating its degree of EMF sensitivity (Section 4). In these situations, it is necessary to check MRI compatibility (integrity of the RF field in the presence of inserted objects) and the insensitivity of onboard devices to EMF. This can be achieved by comparing the field distributions without and with disturbing elements. The field constancy in the case of exposed shielded onboard devices will be checked inside the device without and with exposure.

Indeed, for a given field source value E_e corresponding to J_e, the solution of Equations (1)–(4) in the discretized elements will give the induced values of the EMFs, E, B and J in each element. The obtained distribution of these EMFs allows EMC control. The source E_e

corresponds to RF source B_1 in the case of MRI or to the exposure of external EMF in the case of onboard devices. The solution domains will be, respectively, the birdcage in the tunnel of the MRI or the onboard device structure. The checked EMC control will be practiced on the induced EMFs' distributions in each of these solution domains. This will consist of the verification of the integrity (constancy) of the field distributions in the solution domains regarding object insertion in the MRI case or EMF exposure in the onboard device case. Such EMC controls could be carried out on the checked instrument isolated to guarantee its proper functioning. However, these devices (MRI or onboard devices) normally work close to body tissues and can interact together. Such interaction can affect the device behavior as well as the tissues and in certain situations, we may need to consider the body tissue in the solution domain.

5.2. Body Numerical Virtual Models

As discussed in the last sections, two categories of healthcare medical devices are affected by EMF-related disturbances and EMC control to monitor these disturbances. Such EMC monitoring can be carried out for isolated disturbed elements in the absence of living human tissues undergoing treatment. However, such control can take into account real environmental conditions and, in particular, the effects of the patient's bodily presence. This could be achieved experimentally while avoiding any risk to the patient by using a physical copy of the body (phantom) constructed from materials reflecting the body's true biological possessions. The same consideration of real conditions can be practiced in an EMC analysis by mathematical modeling via digital control, taking into account virtual copies of physical bodies (virtual phantom). Note that such virtual representations also make it possible to identify side effects on health due to medical devices disrupted by EMFs.

Much research has been carried out on building models of human bodies. In general, these models require detailed data on the dielectric properties of living tissues for different parts of the body. These can be obtained from permittivity and electrical conductivity measurement data as a function of frequency. Thus, it is possible to construct an accurate and high-resolution tissue model [123–127]. Such a model corresponds well with local discretized numerical methods used for the calculation of induced fields in medical devices and human tissues.

5.3. Qualitative Methodology Case Study Example

A simple case was considered to demonstrate the conferred control strategy of compatibility of matters introduced into the birdcage RF coil located inside an MRI tunnel. The concerned geometry consists of a birdcage of a 30 cm diameter and 30 cm length, positioned in a 60-cm-diameter tunnel. The checked materials are of a cubic form of a 5 cm edge inserted in the birdcage coil center. We take an RF field in the birdcage coil of 63.87 MHz consistent with the frequency f_L (for B_0 = 1.5 T), which is tuned to the central value of the geometry. The RF field distribution is computed in the tunnel based on 3D discretization of the **E** field on edge finite elements associated with appropriate boundary conditions. Actually, to take into account the skin effect in case of conducting parts, a surface impedance boundary condition is used. The system's boundary (tunnel bore) is considered as a perfect conductor in which the field cannot penetrate. Computations have been carried out for the reference case without material and for different matters. Figure 4 illustrates a comparison of the reference case (a), aluminum conductor (b) and PZT piezoelectric matter (c). The characteristics of the piezoelectric matter are μ_r = 1.0, ε_r = [450 990 990] and σ = 0 S/m. Note that the relative permittivity is given by an anisotropic vector where the value in the polarization direction is smaller compared to the other directions. The characteristics of the conductor are μ_r = 1.0, ε_r = 1.0 and $\sigma = 3.77 \times 10^7$ S/m.

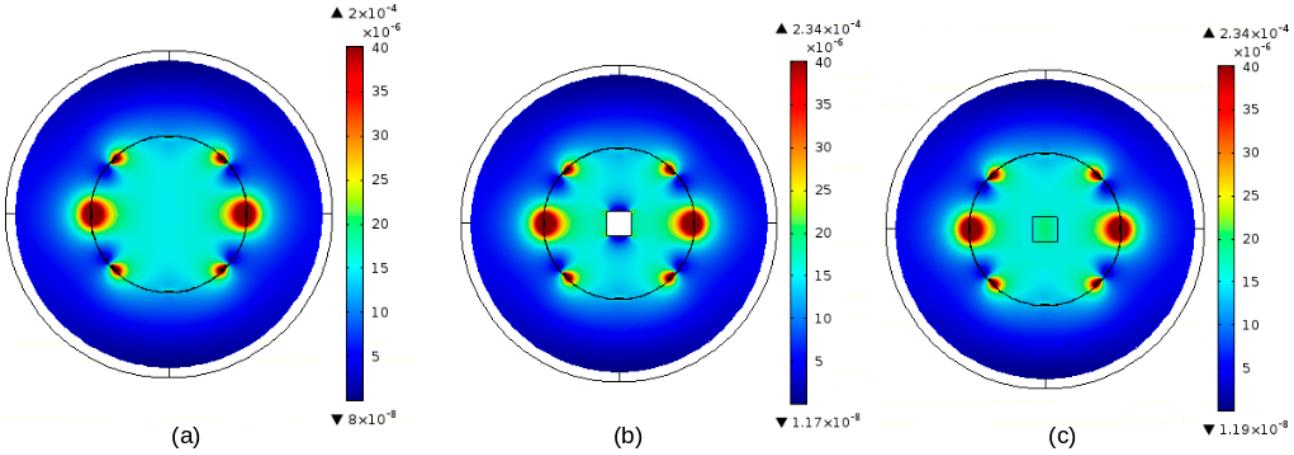

Figure 4. RF B_1 field (vertically directed) distribution in the axial cross section of the birdcage in the tunnel: (**a**) reference case, (**b**) conductor, (**c**) piezoelectric matter.

As expected, as shown in Figure 4, dielectric piezoelectric matter shows no effect while conducting material that alters the distribution of the field. We have chosen to illustrate the conductor case due to the fact that the perturbation is related to the orientation of the introduced matter and its surface perpendicular to the RF B_1 field axis (see Section 3.1). Note that the currents induced by a field in a conductor are developed in the section of the conductor perpendicular to the direction of the field.

Notice that the field distributions of Figure 4a–c are obtained for identical input conditions; therefore, they suggest a behavioral evocation. COMSOL software was used for the problem simulation.

Now, the present EMC analysis in MRI illuminates a procedure for inspection of disturbances in image-guided exercises.

6. Discussion

In this contribution, the analysis and evaluation carried out with a view of monitoring disturbances due to EMF noise in medical devices working close to living tissues have demonstrated that such a subject is fully significant. At this stage, several issues are worth discussing:

- Implanted treatments are considered in Sections 3 and 4 in two different situations. This includes the case of implanted treatment that needs movement or location control with augmented accuracy, which has been considered in Section 3 regarding image-assisted treatments. The other concerned static passive and active implanted devices considered in Section 4 are in regard to onboard autonomous devices. The difference between these two cases in relation to the disturbance of EMF noise is that in the first, the procedure implemented with the treatment could disrupt the functioning of the assisting MRI, while in the second, an external exposure source could disrupt the operation of the implanted onboard device.
- As discussed in Section 5.2, regarding EMC control using a mathematical modeling analysis, the incorporation of virtual phantoms representing the patient's tissues involved in the medical treatment using the disturbed device might be necessary. This allows taking into account more realistic operating conditions for medical devices under control. Such a check is provided separately to guarantee the proper functioning of the device. However, in certain cases, this functioning could be linked to neighboring tissues and, in particular, under exposure to EMF. In fact, EMF exposure can produce biological thermal effects in living tissues that may be greater with longer durations. Under such conditions, consideration of virtual phantoms in the control model permits the consideration of an unshielded device malfunction effect associated with a biological thermal effect due to EMF exposure. It should be noted that such

a malfunction could lead to tissue heating caused by heated metal parts involved in the device. Additionally, in the case of shielded onboard devices, the shielding materials are often electrically conductive. Even if the device in this case is protected from exposure to EMFs, the induced currents can heat the metal of the shield, which can cause tissue heating. This thermal behavior mainly concerns onboard devices, which may be subject to long EMF exposure intervals. In the case of image-assisted treatments, it may be noted that the MRI RF field exposure to the body tissues occurs for short intervals.

- In the case of onboard devices exposed to EMF waves, we consider four options for exposure. The first concerns devices made of materials insensitive to EMF (no magnetic or conductive material); in this case, exposure to electromagnetic fields will not disrupt the device but can only affect living tissue. The second case concerns devices comprising materials sensitive to EMF (magnetic and/or conductive material). In such a case, the device will be disturbed by EMF exposure and the tissues will be affected directly by the exposure and indirectly by the disturbed device. The third case concerns the last device but shielded with a simple conductive material. In this case, the exposure will not disrupt the operation of the device, but the tissues will be affected directly by the exposure and indirectly by the shield. The fourth option concerns the adaptation of the conductive nature of the shielding. Indeed, electromagnetic radiation shielding is corroborated by two basic loss types, reflection and absorption losses. In the occurrence of a conductive shield, the surface electric impedance can be written as a function of electromagnetic parameters, as $Z_s = (\omega \cdot \mu/\sigma)^{1/2}$. This impedance is much lower than the free space impedance $Z_0 = (\mu_0/\varepsilon_0)^{1/2} \approx 376.7$ ohm. If a plane field wave hits the shield, a high impedance discrepancy triggers strong reflections. The surviving field is conveyed across the shield after part absorption. The radiated field with elevated frequencies, e.g., RF, only infiltrates the close surface section of a conductor, due to a skin effect. The depth of penetration δ (skin depth) can be expressed as $\delta = (\omega \cdot \mu \cdot \sigma/2)^{-1/2}$. Note that this expression is only utilizable if δ is superior to the mean free path of an electron within the material. Regarding the losses due to reflection and absorption, the first diminishes with the frequency while the second, which is correlated to the thickness of the shield, rises with the frequency. The total sum of these losses represents the total shielding (screening) effectiveness (SE), which is termed as the ratio of strengths of EMFs without and with the shielded device. Thus, in the last option regarding the adaptation of the conductive nature of the shielding, the use of multifunctional matched materials for low-reflectivity EMI shielding can provide improved protection. The material tailoring can reduce the strong EM reflection caused by the high conductivity of the material. Additionally, a specific manufacturing process can reduce the reflected power coefficient of the material, added to reduced losses and improved thermal insulation and environmentally friendly shielding materials; see, e.g., [128–130]. In conclusion, only a device made from EMF-insensitive materials or elegantly shielded, and exposed to EMF for a short interval, can be safe.
- In case of continuous or prolonged exposure to EMF waves of onboard devices working near human tissues, EMC monitoring of the device must be accompanied by an assessment of tissue heating. This can be accomplished by a coupled solution of the EMF-bio thermal heat transfer equations [33,102,131]. Indeed, the thermal behavior of tissues can be determined from the EMF power loss dissipated, in the tissues on one side and in conductive metals of unshielded devices or in simple conductive shields of devices on the other side. These dissipated losses can be calculated from the induced EMFs obtained from the 3D solution of Equations (1)–(4). The value of this EMF power loss can be used as the input heat source in the 3D solution of the heat transfer equation. Such a solution provides access to the ΔT distribution of the temperature rise in the solution domain of concern. The thermal behavior in living tissues is governed by Penne's bio-heat equation [33,102,131]. Note that dissipated

power density $P_d = \sigma \cdot E^2/2$ is in conductors and $P_d = \omega \cdot \varepsilon'' \cdot E^2/2$ in is dielectrics (tissues), where E is the absolute peak value of the electric field strength in $V \cdot m^{-1}$, ε'' is the imaginary part of the complex permittivity of the absorbing material in $F \cdot m^{-1}$ and the dissipated power density P_d is in $W \cdot m^{-3}$. Penne's bio-heat equation is given with $c\ \rho\ \partial T/\partial t = \nabla \cdot (k\ \nabla T) + P_d + q_{met} - C_b\ \rho_b\ \omega_b\ (T - T_b)$. In this equation, c is the specific heat in $J \cdot kg^{-1} \cdot {}^\circ C^{-1}$, k is thermal conductivity in $W \cdot m^{-1} \cdot {}^\circ C^{-1}$ and ρ is density in $kg \cdot m^{-3}$ of the substance. T is local temperature in °C, q_{met} is the basal metabolic heat source in $W \cdot m^{-3}$, c_b is blood-specific heat in $J \cdot kg^{-1} \cdot {}^\circ C^{-1}$, ρ_b is blood density in $kg \cdot m^{-3}$, ω_b is the blood perfusion rate in 1/s and T_b is the blood temperature in °C. The term $\nabla \cdot (k \nabla T)$ symbolizes the heat equation in a differential form. Figure 5 illustrates the control strategies for onboard devices in case of exposure to EMF, involving the exposure interval, device integrity and temperature rise in living body tissues.

- Following the example given in Section 5.3, concerning the distribution of the RF field under the effect of the introduction of external materials, certain details deserve to be underlined. The first concerns the characteristics of matter affecting the modification of the field distribution. These involve, in addition to physical behavior, the size, shape and orientation in space in relation to the direction of the field. The size is directly related to the importance of the disturbance of the field distribution. For very small sizes, generally the disturbances could be negligible or easily compensated. Magnetic materials are the most disruptive around its volume and should be avoided. Dielectric materials are practically non-disruptive. Disturbances linked to conductive materials are strongly linked to shape and spatial orientation. The larger the surface of the conductor perpendicular to the axis of B_1, the greater the induced eddy currents and associated field disturbances will be. Thus, a conductive sheet of insignificant thickness positioned parallel to the field will hardly disturb the field distribution. This observation may facilitate the use of thin electrodes for properly positioned devices in the RF coil without field disturbance. Typical examples of non-disruptive field distribution could be piezoelectric sensors and actuators composed of piezoelectric stacks, which behave dielectrically, equipped with thin sheet electrodes, which can be controlled to be parallel to the field direction [46–55,121].

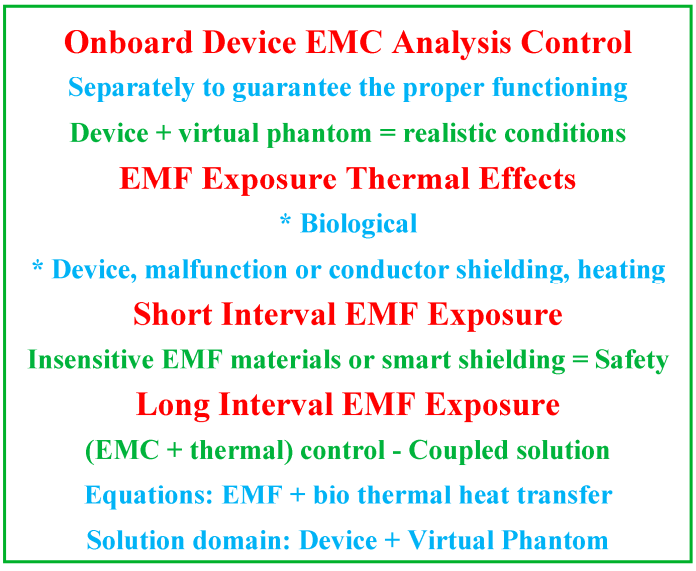

(**a**)

Figure 5. *Cont.*

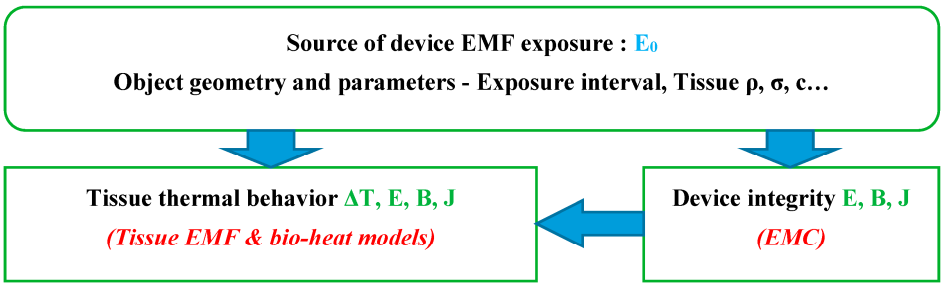

(**b**)

Figure 5. Illustration of control strategies for onboard devices in case of exposure to EMF. (**a**) Summarizing diagram of exposure behaviors, (**b**) schemes for controlling the device integrity and the temperature rise in living body tissues.

7. Conclusions

In this contribution, the evaluation, discussion and analysis of disturbances due to EMF noise of medical devices working near living tissues and the corresponding functional EMC control of these devices were carried out. The analysis of the different interests covered in this review revealed that there is persistent development in this area. The important elements raised by this theme are diverse, the most important of which are summarized as follows.

An important goal of healthcare management could be to ensure the proper functioning of medical instruments working close to the patient's body tissues and enable their protection by monitoring potential disturbances. Thanks to these commitments, different health recommendations can be advocated:

- Image-assisted robotics involving MRI and piezoelectric devices offer support for patient well-being.
- Conductive materials can be introduced into the MRI subject to particular shapes and spatial orientation in addition to EMC verification.
- Embedded devices constructed from EMF-insensitive materials or intelligently shielded can be used safely with short EMF exposure intervals.
- In case of continuous or prolonged EMF exposure, the increase in body tissue temperature must be supervised in addition to EMC monitoring.
- The use of virtual tissue models in EMC testing allows for more realistic evaluation capabilities.

From the above points, we see that alternative measures to alleviate the EMF exposure problem of medical equipment working near-body could be the use of MRI-compatible materials and onboard devices built from EMF-insensitive matters or smartly shielded.

In conclusion, EMF can disrupt medical devices working near living tissues by altering their functioning. These devices are mainly MRI and onboard devices. The resulting EMF disturbances would be deterioration of the MRI image and malfunction of onboard devices. Such disturbances could be verified by EMC monitoring. Correction of these disturbances could be achieved by using MRI-compatible materials in the imager and onboard devices constructed from EMF-insensitive materials or intelligently shielded. The results of these solutions could again be monitored by EMC verification.

Funding: This research received no external funding.

Conflicts of Interest: The authors declare no conflict of interest.

References

1. Petroulakis, N.; Mattsson, M.O.; Chatziadam, P.; Simko, M.; Gavrielides, A.; Yiorkas, A.M.; Zeni, O.; Scarfi, M.R.; Soudah, E.; Otin, R.; et al. NextGEM: Next-Generation Integrated Sensing and Analytical System for Monitoring and Assessing Radiofrequency Electromagnetic Field Exposure and Health. *Int. J. Environ. Res. Public Health* **2023**, *20*, 6085. [CrossRef]
2. Henschenmacher, B.; Bitsch, A.; de Las Heras Gala, T.; Forman, H.J.; Fragoulis, A.; Ghezzi, P.; Kellner, R.; Koch, W.; Kuhne, J.; Sachno, D.; et al. The effect of radiofrequency electromagnetic fields (RF-EMF) on biomarkers of oxidative stress in vivo and in vitro: A protocol for a systematic review. *Environ. Int.* **2022**, *158*, 106932. [CrossRef]
3. Hamed, T.; Maqsood, M. SAR Calculation & Temperature Response of Human Body Exposure to Electromagnetic Radiations at 28, 40 and 60 GHz mm Wave Frequencies. *Prog. Electromagn. Res. M* **2018**, *73*, 47–59. [CrossRef]
4. Lagorio, S.; Blettner, M.; Baaken, D.; Feychting, M.; Karipidis, K.; Loney, T.; Orsini, N.; Röösli, M.; Paulo, M.S.; Elwood, M. The effect of exposure to radiofrequency fields on cancer risk in the general and working population: A protocol for a systematic review of human observational studies. *Environ. Int.* **2021**, *157*, 106828. [CrossRef] [PubMed]
5. Romeo, S.; Zeni, O.; Sannino, A.; Lagorio, S.; Biffoni, M.; Scarfì, M.R. Genotoxicity of radiofrequency electromagnetic fields: Protocol for a systematic review of in vitro studies. *Environ. Int.* **2021**, *148*, 106386. [CrossRef] [PubMed]
6. Pophof, B.; Burns, J.; Danker-Hopfe, H.; Dorn, H.; Egblomasse-Roidl, C.; Eggert, T.; Fuks, K.; Henschenmacher, B.; Kuhne, J.; Sauter, C.; et al. The effect of exposure to radiofrequency electromagnetic fields on cognitive performance in human experimental studies: A protocol for a systematic review. *Environ. Int.* **2021**, *157*, 106783. [CrossRef] [PubMed]
7. Kovács, A.; Bischoff, P.; Haddad, H.; Kovács, G.; Schaefer, A.; Zhou, W.; Pinkawa, M. Personalized Image-Guided Therapies for Local Malignencies: Interdisciplinary Options for Interventional Radiology and Interventional Radiotherapy. *Front. Oncol.* **2021**, *11*, 616058. [CrossRef] [PubMed]
8. Zhao, J.; Zhi, Z.; Zhang, H.; Zhao, J.; Di, Y.; Xu, K.; Ma, C.; Liu, Z.; Sui, A.; Wang, J. Efficacy and safety of CT guided 125I brachytherapy in elderly patients with non small cell lung cancer. *Oncol. Lett.* **2020**, *20*, 183–192. [CrossRef] [PubMed]
9. Park, B.K. Ultrasound-guided genitourinary interventions: Principles and techniques (Review Article). *Ultrasonography* **2017**, *36*, 336–348. [CrossRef]
10. Pinto, P.A.; Chung, P.H.; Rastinehad, A.R.; Baccala, A.A., Jr.; Kruecker, J.; Benjamin, C.J.; Xu, S.; Yan, P.; Kadoury, S.; Chua, C.; et al. Magnetic resonance imaging/ultrasound fusion guided prostate biopsy improves cancer detection following transrectal ultrasound biopsy and correlates with multiparametric magnetic resonance imaging. *J. Urol.* **2011**, *186*, 1281–1285. [CrossRef]
11. Fiard, G.; Hohn, N.; Descotes, J.L.; Rambeaud, J.J.; Troccaz, J.; Long, J.A. Targeted MRI-guided prostate biopsies for the detection of prostate cancer: Initial clinical experience with real-time 3-dimensional transrectal ultrasound guidance and magnetic resonance/transrectal ultrasound image fusion. *Urology* **2013**, *81*, 1372–1378. [CrossRef]
12. Veltri, A.; Garetto, I.; Pagano, E.; Tosetti, I.; Sacchetto, P.; Fava, C. Percutaneous RF thermal ablation of renal tumors: Is US guidance really less favorable than other imaging guidance techniques? *Cardiovasc. Intervent. Radiol.* **2009**, *32*, 76–85. [CrossRef] [PubMed]
13. Bassignani, M.; Moore, Y.; Watson, L.; Theodorescu, D. Pilot experience with real-time ultrasound guided percutaneous renal mass cryoablation. *J. Urol.* **2004**, *171*, 1620–1623. [CrossRef]
14. Guk, K.; Han, G.; Lim, J.; Jeong, K.; Kang, T.; Lim, E.-K.; Jung, J. Evolution of Wearable Devices with Real-Time Disease Monitoring for Personalized Healthcare. *Nanomaterials* **2019**, *9*, 813. [CrossRef]
15. Xin, Y.; Liu, T.; Sun, H.; Xu, Y.; Zhu, J.; Qian, C.; Lin, T. Recent progress on the wearable devices based on piezoelectric sensors. *Ferroelectrics* **2018**, *531*, 102–113. [CrossRef]
16. Yetisen, A.K.; Martinez-Hurtado, J.L.; Ünal, B.; Khademhosseini, A.; Butt, H. Wearables in Medicine. *Adv. Mater.* **2018**, *30*, 1706910. [CrossRef]
17. Sener, T.; Haenen, W.; Smits, P.; Hans, G.H. Large-scale real-life implementation of technology-enabled care to maximize hospitals' medical surge preparedness during future infectious disease outbreaks and winter seasons: A viewpoint. *Front. Public Health* **2023**, *11*, 1149247. [CrossRef]
18. Navarro-Valverde, C.; Ramos-Maqueda, J.; Romero-Reyes, M.J.; Esteve-Ruiz, I.; García-Medina, D.; Pavón-Jiménez, R.; Rodríguez-Gómez, C.; Leal-del-Ojo, J.; Cayuela, A.; Molano-Casimiro, F.J. Magnetic resonance imaging in patients with cardiac implantable electronic devices: A prospective study. *Magn. Reson. Imaging* **2022**, *91*, 9–15. [CrossRef]
19. Hirano, M.; Muto, Y.; Kuroda, M.; Fujiwara, Y.; Sasaki, T.; Kuroda, K.; Kamizaki, R.; Imajoh, S.; Tanabe, Y.; Al-Hammad, W.E.; et al. Quantitative evaluation of the reduction of distortion and metallic artifacts in magnetic resonance images using the multiacquisition variable resonance image combination selective sequence. *Exp. Ther. Med.* **2023**, *25*, 109. [CrossRef] [PubMed]
20. Amann, N.; Johnson, S.; Chagarlamudi, K.; Gupta, A.; Faraji, N. Scheduling Musculoskeletal MRI for Patients with Metallic Hardware: Initial Observations on Decreasing Nondiagnostic and Repeat Examinations at a Multisite Academic Medical Center. *Curr. Probl. Diagn. Radiol.* **2023**, *52*, 327–329. [CrossRef] [PubMed]
21. Fujiwara, Y.; Sasaki, T.; Muto, Y.; Hirano, M.; Kamizaki, R.; Murakami, K.; Miura, N.; Fujibuchi, Y.; Ohmukai, N.; Ueda, N.; et al. Multiacquisition Variable-Resonance Image Combination Selective Can Improve Image Quality and Reproducibility for Metallic Implants in the Lumbar Spine. *Acta Med. Okayama* **2021**, *75*, 187–197. [CrossRef] [PubMed]
22. Choo, H.J.; Lee, S.J.; Lee, Y.H. Metallic Artifacts on MR Imaging and Methods for Their Reduction. *Taehan Yongsang Uihakhoe chi* **2020**, *81*, 41–57. [CrossRef] [PubMed]

23. Chinzei, K.; Kikinis, R.; Jolesz, F.A. MR compatibility of mechatronic devices: Design criteria. In *Medical Image Computing and Computer-Assisted Intervention—MICCAI'99*; Springer: Berlin/Heidelberg, Germany, 1999; Volume 1679, pp. 1020–1030.
24. Tsekos, N.V.; Khanicheh, A.; Christoforou, E.; Mavroidis, C. Magnetic resonance-compatible robotic and mechatronics systems for image guided interventions and rehabilitation: A Review Study. *Annu. Rev. Biomed. Eng.* **2007**, *9*, 351–387. [CrossRef]
25. Khairi, R.; Razek, A.; Bernard, L.; Corcolle, R.; Bernard, Y.; Pichon, L.; Poirier-Quinot, M.; Ginefri, J.C. EMC analysis of MRI environment in view of Optimized performance and cost of image guided interventions. *Int. J. Appl. Electromagn. Mech.* **2016**, *51*, S67–S74. [CrossRef]
26. Su, H.; Kwok, K.W.; Cleary, K.; Iordachita, I.; Cavusoglu, M.C.; Desai, J.P.; Fischer, G.S. State of the art and future opportunities in MRI-guided robot-assisted surgery and interventions. *Proc. IEEE* **2022**, *110*, 968–992. [CrossRef]
27. Razek, A. Towards an image-guided restricted drug release in friendly implanted therapeutics. *Eur. Phys. J. Appl. Phys.* **2018**, *82*, 31401. [CrossRef]
28. Velazco Garcia, J.D.; Navkar, N.V.; Gui, D.; Morales, C.M.; Christoforou, E.G.; Ozcan, A.; Abinahed, J.; Al-Ansari, A.; Webb, A.; Seimenis, I.; et al. A Platform Integrating Acquisition, Reconstruction, Visualization, and Manipulator Control Modules for MRI-Guided Interventions. *J. Digit. Imaging* **2019**, *32*, 420–432. [CrossRef]
29. Razek, A. Assessment of Supervised Drug Release in Cordial Embedded Therapeutics. *Athens J. Technol. Eng.* **2019**, *6*, 77–91. [CrossRef]
30. Chakrabarti, S.; Biswas, N.; Jones, L.D.; Kesari, S.; Ashili, S. Smart Consumer Wearables as Digital Diagnostic Tools: A Review. *Diagnostics* **2022**, *12*, 2110. [CrossRef]
31. Escobar-Linero, E.; Muñoz-Saavedra, L.; Luna-Perejón, F.; Sevillano, J.L.; Domínguez-Morales, M. Wearable Health Devices for Diagnosis Support: Evolution and Future Tendencies. *Sensors* **2023**, *23*, 1678. [CrossRef]
32. Devi, D.H.; Duraisamy, K.; Armghan, A.; Alsharari, M.; Aliqab, K.; Sorathiya, V.; Das, S.; Rashid, N. 5G Technology in Healthcare and Wearable Devices: A Review. *Sensors* **2023**, *23*, 2519. [CrossRef]
33. Razek, A. Biological and Medical Disturbances Due to Exposure to Fields Emitted by Electromagnetic Energy Devices—A Review. *Energies* **2022**, *15*, 4455. [CrossRef]
34. Sato, Y.; Takeuchi, T.; Fuju, A.; Takahashi, M.; Hashimoto, M.; Okawa, R.; Hayashi, N. MRI safety for leave-on powdered hair thickeners under 1.5-T and 3.0-T MRI: Measurement of deflection force, MRI artifact, and evaluation of preexamination screening. *Phys. Eng. Sci. Med.* **2023**, *46*, 915–924. [CrossRef]
35. Akdogan, G.; Istanbullu, O. Analysing the effects of metallic biomaterial design and imaging sequences on MRI interpretation challenges due to image artefacts. *Phys. Eng. Sci. Med.* **2022**, *45*, 1163–1174. [CrossRef]
36. Germann, C.; Nanz, D.; Sutter, R. Magnetic Resonance Imaging Around Metal at 1.5 Tesla: Techniques from Basic to Advanced and Clinical Impact. *Investig. Radiol.* **2021**, *56*, 734–748. [CrossRef]
37. Germann, C.; Falkowski, A.L.; von Deuster, C.; Nanz, D.; Sutter, R. Basic and Advanced Metal-Artifact Reduction Techniques at Ultra-High Field 7-T Magnetic Resonance Imaging-Phantom Study Investigating Feasibility and Efficacy. *Investig. Radiol.* **2022**, *57*, 387–398. [CrossRef]
38. Inaoka, T.; Kitamura, N.; Sugeta, M.; Nakatsuka, T.; Ishikawa, R.; Kasuya, S.; Sugiura, Y.; Nakajima, A.; Nakagawa, K.; Terada, H. Diagnostic Value of Advanced Metal Artifact Reduction Magnetic Resonance Imaging for Periprosthetic Joint Infection. *J. Comput. Assist. Tomogr.* **2022**, *46*, 455–463. [CrossRef]
39. Haskell, M.W.; Nielsen, J.F.; Noll, D.C. Off-resonance artifact correction for MRI: A review. *NMR Biomed.* **2023**, *36*, e4867. [CrossRef]
40. Spronk, T.; Kraff, O.; Kreutner, J.; Schaefers, G.; Quick, H.H. Development and evaluation of a numerical simulation approach to predict metal artifacts from passive implants in MRI. *Magma* **2022**, *35*, 485–497. [CrossRef]
41. Farooq, M.U.; Ko, S.Y. A Decade of MRI Compatible Robots: Systematic Review. *Trans. Robot.* **2023**, *39*, 862–884. [CrossRef]
42. Farooq, M.U.; Ko, S.Y.; Seung, S.; Kim, C.; Cha, K.; Oh, S.S.; You, H. An MRI-compatible endonasal surgical robotic system: Kinematic analysis and performance evaluation. *Mechatronics* **2023**, *94*, 103029. [CrossRef]
43. Manjila, S.; Rosa, B.; Price, K.; Manjila, R.; Mencattelli, M.; Dupont, P.E. Robotic Instruments Inside the MRI Bore: Key Concepts and Evolving Paradigms in Imaging-enhanced Cranial Neurosurgery. *World Neurosurg.* **2023**, *176*, 127–139. [CrossRef] [PubMed]
44. Zhao, Z.; Carvalho, P.A.; Tang, H.; Pooladvand, K.; Gandomi, K.Y.; Nycz, C.J.; Furlong, C.; Fischer, G.S. Preliminary Characterization of a Plastic Piezoelectric Motor Stator Using High-Speed Digital Holographic Interferometry. In *Advancement of Optical Methods & Digital Image Correlation in Experimental Mechanics*; Lin, M.T., Furlong, C., Hwang, C.H., Eds.; Conference Proceedings of the Society for Experimental Mechanics Series; Springer: Cham, Switzerland, 2021. [CrossRef]
45. Carvalho, P.A.; Tang, H.; Razavi, P.; Pooladvand, K.; Castro, W.C.; Gandomi, K.Y.; Zhao, Z.; Nycz, C.J.; Furlong, C.; Fischer, G.S. Study of MRI Compatible Piezoelectric Motors by Finite Element Modeling and High-Speed Digital Holography. In *Advancements in Optical Methods & Digital Image Correlation in Experimental Mechanics*; Lin, M.T., Furlong, C., Hwang, C.H., Eds.; Conference Proceedings of the Society for Experimental Mechanics Series; Springer: Cham, Switzerland, 2020; Volume 3. [CrossRef]
46. Zhang, S.J.; Liu, Y.; Deng, J.; Gao, X.; Li, J.; Wang, W.Y.; Xun, M.X.; Ma, X.F.; Chang, Q.B.; Liu, J.K.; et al. Piezo robotic hand for motion manipulation from micro to macro. *Nat. Commun.* **2023**, *14*, 500. [CrossRef] [PubMed]
47. Mohith, S.; Upadhya, A.R.; Navin, K.P.; Kulkarni, S.M.; Rao, M. Recent trends in piezoelectric actuators for precision motion and their applications: A review. *Smart Mater. Struct.* **2020**, *30*, 013002. [CrossRef]

48. Gao, X.; Yang, J.; Wu, J.; Xin, X.; Li, Z.; Yuan, X.; Shen, X.; Dong, S. Piezoelectric Actuators and Motors: Materials, Designs, and Applications. *Adv. Mater. Technol.* **2020**, *5*, 1900716. [CrossRef]
49. Qiao, G.; Li, H.; Lu, X.; Wen, J.; Cheng, T. Piezoelectric stick-slip actuators with flexure hinge mechanisms: A review. *J. Intell. Mater. Syst. Struct.* **2022**, *33*, 1879–1901. [CrossRef]
50. Liu, J.; Gao, X.; Jin, H.; Ren, K.; Guo, J.; Qiao, L.; Qiu, C.; Chen, W.; He, Y.; Dong, S.; et al. Miniaturized electromechanical devices with multi-vibration modes achieved by orderly stacked structure with piezoelectric strain units. *Nat. Commun.* **2022**, *13*, 6567. [CrossRef]
51. Fu, D.K.; Fan, P.Q.; Yuan, T.; Wang, Y.S. A novel hybrid mode linear ultrasonic motor with double driving feet. *Rev. Sci. Instrum.* **2022**, *93*, 025003. [CrossRef]
52. Li, Z.; Guo, Z.; Han, H.; Su, Z.; Sun, H. Design and characteristic analysis of multi-degree-of-freedom ultrasonic motor based on spherical stator. *Rev. Sci. Instrum.* **2022**, *93*, 025004. [CrossRef] [PubMed]
53. Wang, S.; Zhou, S.; Zhang, X.; Xu, P.; Zhang, Z.; Ren, L. Bionic Stepping Motors Driven by Piezoelectric Materials. *J. Bionic Eng.* **2023**, *20*, 858–872. [CrossRef]
54. Hernandez, C.; Bernard, Y.; Razek, A. Design and manufacturing of a piezoelectric traveling-wave pumping device. *IEEE Trans. Ultrason. Ferroelectr. Freq. Control* **2013**, *60*, 1949–1956. [CrossRef]
55. Yang, Z.; Li, X.; Tang, J.; Huang, H.; Zhao, H.; Cheng, Y.; Liu, S.; Li, C.; Xiong, M. A Bionic Stick–Slip Piezo-Driven Positioning Platform Designed by Imitating the Structure and Movement of the Crab. *J. Bionic Eng.* **2023**, *20*, 2590–2600. [CrossRef]
56. Virtanen, J. Enhancing the Compatibility of Surgical Robots with Magnetic Resonance Imaging. Ph.D. Thesis, University of Oulu, Oulu, Finland, 2006. Available online: http://urn.fi/urn:isbn:9514280660 (accessed on 1 November 2023).
57. Tada, M.; Sasaki, S.; Ogasawara, T. Development of an optical 2-axis force sensor usable in MRI environments. In Proceedings of the SENSORS, 2002 IEEE, Orlando, FL, USA, 12–14 June 2002; Volume 2, pp. 984–989. [CrossRef]
58. Tada, M.; Kanade, T. An MR-Compatible Optical Force Sensor for Human Function Modeling. In *Medical Image Computing and Computer-Assisted Intervention—MICCAI 2004. Lecture Notes in Computer Science*; Barillot, C., Haynor, D.R., Hellier, P., Eds.; Springer: Berlin/Heidelberg, Germany, 2004; Volume 3217. [CrossRef]
59. Jolesz, F.A.; Morrison, P.R.; Koran, S.J.; Kelley, R.J.; Hushek, S.G.; Newman, R.W.; Fried, M.P.; Melzer, A.; Seibel, R.M.; Jalahej, H. Compatible instrumentation for intraoperative MRI: Expanding resources. *J. Magn. Reson. Imaging* **1998**, *8*, 8–11. [CrossRef] [PubMed]
60. Shellock, F.G. *Pocket Guide to MR Procedures and Metallic Objects: Update 1998*; Lippincott-Raven Publishers: Philadelphia, PA, USA, 1998; Available online: https://archive.org/details/pocketguidetomrp0000shel_y5n3 (accessed on 1 November 2023).
61. Schenck, J.F. The role of magnetic susceptibility in magnetic resonance imaging: MRI magnetic compatibility of the first and second kinds. *Med. Phys.* **1996**, *23*, 815–850. [CrossRef] [PubMed]
62. Traverson, M.; Heiden, M.; Stanciu, L.A.; Nauman, E.A.; Jones-Hall, Y.; Breur, G.J. In Vivo Evaluation of Biodegradability and Biocompatibility of Fe30Mn Alloy. *Vet. Comp. Orthop. Traumatol.* **2018**, *31*, 10–16. [CrossRef] [PubMed]
63. Wang, Y.; Venezuela, J.; Dargusch, M. Biodegradable shape memory alloys: Progress and prospects. *Biomaterials* **2021**, *279*, 121215. [CrossRef]
64. Li, H.; Lin, G.; Wang, P.; Huang, J.; Wen, C. Nutrient alloying elements in biodegradable metals: A review. *J. Mater. Chem. B* **2021**, *9*, 9806–9825. [CrossRef]
65. Rabeeh, V.P.M.; Hanas, T. Progress in manufacturing and processing of degradable Fe-based implants: A review. *Prog. Biomater.* **2022**, *11*, 163–191. [CrossRef] [PubMed]
66. Babacan, N.; Kochta, F.; Hoffmann, V.; Gemming, T.; Kühn, U.; Giebeler, L.; Gebert, A.; Hufenbach, J. Effect of silver additions on the microstructure, mechanical properties and corrosion behavior of biodegradable Fe-30Mn-6Si. *Mater. Today Commun.* **2021**, *28*, 102689. [CrossRef]
67. Tai, C.-C.; Lo, H.-L.; Liaw, C.-K.; Huang, Y.-M.; Huang, Y.-H.; Yang, K.-Y.; Huang, C.-C.; Huang, S.-I.; Shen, H.-H.; Lin, T.-H.; et al. Biocompatibility and Biological Performance Evaluation of Additive-Manufactured Bioabsorbable Iron-Based Porous Suture Anchor in a Rabbit Model. *Int. J. Mol. Sci.* **2021**, *22*, 7368. [CrossRef]
68. Bakhsheshi-Rad, H.R.; Najafinezhad, A.; Hadisi, Z.; Iqbal, N.; Daroonparvar, M.; Sharif, S.; Ismail, A.F.; Akbari, M.; RamaKrishna, S.; Berto, F. Characterization and biological properties of nanostructured clinoenstatite scaffolds for bone tissue engineering applications. *Mater. Chem. Phys.* **2021**, *259*, 123969. [CrossRef]
69. Sun, Y.; Chen, L.; Liu, N.; Wang, H.; Liang, C. Laser-modified fe–30mn surfaces with promoted biodegradability and biocompatibility toward biological applications. *J. Mater. Sci.* **2021**, *56*, 13772–13784. [CrossRef]
70. Saliba, L.; Sammut, K.; Tonna, C.; Pavli, F. FeMn and FeMnAg Biodegradable Alloys: An In Vitro And In Vivo Investigation. Available online: https://ssrn.com/abstract=4325636 (accessed on 1 November 2023). [CrossRef]
71. Hao, S.; Yang, T.; Zhang, A.; Wang, P.; Jiang, H.; Shen, D.; Guo, L.; Ye, M. Evaluation of Biodegradable Alloy Fe30Mn0.6N in Rabbit Femur and Cartilage through Detecting Osteogenesis and Autophagy. *BioMed Res Int.* **2023**, *2023*, 3626776. [CrossRef]
72. Biffi, C.A.; Fiocchi, J.; Bregoli, C.; Gambaro, S.; Copes, F.; Mantovani, D.; Tuissi, A. Ultrashort Laser Texturing for Tuning Surface Morphology and Degradation Behavior of the Biodegradable Fe–20Mn Alloy for Temporary Implants. *Adv. Eng. Mater.* **2022**, *24*, 2101496. [CrossRef]
73. Putra, N.E.; Leeflang, M.A.; Taheri, P.; Fratila-Apachitei, L.E.; Mol, J.M.C.; Zhou, J.; Zadpoor, A.A. Extrusion-based 3D printing of ex situ-alloyed highly biodegradable MRI-friendly porous iron-manganese scaffolds. *Acta Biomater.* **2021**, *134*, 774–790. [CrossRef]

74. Soliman, M.M.; Chowdhury, M.E.H.; Khandakar, A.; Islam, M.T.; Qiblawey, Y.; Musharavati, F.; Zal Nezhad, E. Review on Medical Implantable Antenna Technology and Imminent Research Challenges. *Sensors* **2021**, *21*, 3163. [CrossRef] [PubMed]
75. Gupta, A.; Kumar, V.; Bansal, S.; Alsharif, M.H.; Jahid, A.; Cho, H.-S. A Miniaturized Tri-Band Implantable Antenna for ISM/WMTS/Lower UWB/Wi-Fi Frequencies. *Sensors* **2023**, *23*, 6989. [CrossRef]
76. Chowdhury, M.E.H.; Khandakar, A.; Alzoubi, K.; Mansoor, S.; Tahir, A.M.; Reaz, M.B.I.; Al-Emadi, N. Real-Time Smart-Digital Stethoscope System for Heart Diseases Monitoring. *Sensors* **2019**, *19*, 2781. [CrossRef] [PubMed]
77. Moon, K.S.; Lee, S.Q. A Wearable Multimodal Wireless Sensing System for Respiratory Monitoring and Analysis. *Sensors* **2023**, *23*, 6790. [CrossRef] [PubMed]
78. Khan Mamun, M.M.R.; Sherif, A. Advancement in the Cuffless and Noninvasive Measurement of Blood Pressure: A Review of the Literature and Open Challenges. *Bioengineering* **2022**, *10*, 27. [CrossRef] [PubMed]
79. Bhuva, A.N.; Moralee, R.; Brunker, T.; Lascelles, K.; Cash, L.; Patel, K.P.; Lowe, M.; Sekhri, N.; Alpendurada, F.; Pennell, D.J.; et al. Evidence to support magnetic resonance conditional labelling of all pacemaker and defibrillator leads in patients with cardiac implantable electronic devices. *Eur. Heart J.* **2022**, *43*, 2469–2478. [CrossRef]
80. Joo, H.; Lee, Y.; Kim, J.; Yoo, J.S.; Yoo, S.; Kim, S.; Arya, A.K.; Kim, S.; Choi, S.H.; Lu, N.; et al. Soft Implantable Drug Delivery Device Integrated Wirelessly with Wearable Devices to Treat Fatal Seizures. *Sci. Adv.* **2021**, *7*, eabd4639. [CrossRef]
81. Cheng, Y.; Xie, D.; Han, Y.; Guo, S.; Sun, Z.; Jing, L.; Man, W.; Liu, D.; Yang, K.; Lei, D.; et al. Precise management system for chronic intractable pain patients implanted with spinal cord stimulation based on a remote programming platform: Study protocol for a randomized controlled trial (PreMaSy study). *Trials* **2023**, *24*, 580. [CrossRef] [PubMed]
82. Thotahewa, K.M.S.; Redouté, J.; Yuce, M.R. Electromagnetic and thermal effects of IR-UWB wireless implant systems on the human head. In Proceedings of the 2013 35th Annual International Conference of the IEEE Engineering in Medicine and Biology Society (EMBC), Osaka, Japan, 3–7 July 2013; pp. 5179–5182. [CrossRef]
83. Corbett, G.D.; Buttery, P.C.; Pugh, P.J.; Cameron, E.A.B. Endoscopy and implantable electronic devices. *Frontline Gastroenterol.* **2012**, *3*, 72–75. [CrossRef] [PubMed]
84. Pantelopoulos, A.; Bourbakis, N.G. A survey on wearable sensor-based systems for health monitoring and prognosis. *IEEE Trans. Syst. Man Cybern. Part C* **2010**, *40*, 1–12. [CrossRef]
85. Chan, M.; Esteve, D.; Fourniols, J.Y.; Escriba, C.; Campo, E. Smart wearable systems: Current status and future challenges. *Artif. Intell. Med.* **2012**, *56*, 137–156. [CrossRef] [PubMed]
86. Kim, J.; Campbell, A.S.; de Ávila, B.E.; Wang, J. Wearable biosensors for healthcare monitoring. *Nat. Biotechnol.* **2019**, *37*, 389–406. [CrossRef] [PubMed]
87. Khan, Y.; Ostfeld, A.E.; Lochner, C.M.; Pierre, A.; Arias, A.C. Monitoring of vital signs with flexible and wearable medical devices. *Adv. Mater.* **2016**, *28*, 4373–4395. [CrossRef] [PubMed]
88. Patel, S.; Park, H.; Bonato, P.; Chan, L.; Rodgers, M. A review of wearable sensors and systems with application in rehabilitation. *J. Neuroeng. Rehabil.* **2012**, *9*, 1–17. [CrossRef]
89. Hurley, N.C.; Spatz, E.S.; Krumholz, H.M.; Jafari, R.; Mortazavi, B.J. A Survey of Challenges and Opportunities in Sensing and Analytics for Risk Factors of Cardiovascular Disorders. *ACM Trans. Comput. Healthc.* **2021**, *2*, 9–21. [CrossRef]
90. Talal, M.; Zaidan, A.A.; Zaidan, B.B.; Albahri, A.S.; Alamoodi, A.H.; Albahri, O.S.; Alsalem, M.A.; Lim, C.K.; Tan, K.L.; Shir, W.L.; et al. Smart Home-based IoT for Real-time and Secure Remote Health Monitoring of Triage and Priority System using Body Sensors: Multi-driven Systematic Review. *J. Med. Syst.* **2019**, *43*, 42. [CrossRef] [PubMed]
91. Patel, V.; Orchanian-Cheff, A.; Wu, R. Evaluating the Validity and Utility of Wearable Technology for Continuously Monitoring Patients in a Hospital Setting: Systematic Review. *JMIR Mhealth Uhealth* **2021**, *9*, e17411. [CrossRef] [PubMed]
92. Osama, M.; Ateya, A.A.; Sayed, M.S.; Hammad, M.; Pławiak, P.; Abd El-Latif, A.A.; Elsayed, R.A. Internet of Medical Things and Healthcare 4.0: Trends, Requirements, Challenges, and Research Directions. *Sensors* **2023**, *23*, 7435. [CrossRef] [PubMed]
93. *IEC 61000-6-1:2019*; Electromagnetic Compatibility (EMC)—Part 6–1. IEC: Geneva, Switzerland, 2019.
94. *IEC/TS 61000-1-2*; Electromagnetic Compatibility (EMC)—Methodology for the Achievement of the Functional Safety of Electrical and Electronic with Regard to Electromagnetic Phenomena. IEC: Geneva, Switzerland, 2019.
95. CISPR 16-1-1 Specification for Radio Disturbance and Immunity Measuring Apparatus and Methods—Part 1-1: Radio Disturbance and Immunity Measuring Apparatus—Measuring Apparatus. 2019. Available online: https://webstore.iec.ch/publication/60774 (accessed on 5 October 2021).
96. Sabath, F. A systematic approach for electromagnetic interference risk management. *IEEE Electromagn. Compat. Mag.* **2017**, *6*, 99–106. [CrossRef]
97. Jang, J.; Paonni, M.; Eissfeller, B. CW Interference Effects on Tracking Performance of GNSS Receivers. *IEEE Trans. Aerosp. Electron. Syst.* **2012**, *48*, 243–258. [CrossRef]
98. Su, D.; Xie, S.; Chen, A.; Shang, X.; Zhu, K.; Xu, H. Basic emission waveform theory: A novel interpretation and source identification method for electromagnetic emission of complex systems. *IEEE Trans. Electromagn. Compat.* **2018**, *60*, 1330–1339. [CrossRef]
99. Hoijer, M. Including Directivity in Reverberation Chamber Radiated Susceptibility Testing. *IEEE Trans. Electromagn. Compat.* **2011**, *53*, 283–287. [CrossRef]
100. Spadacini, G.; Grassi, F.; Pignari, S.A.; Bisognin, P.; Piche, A. Bulk Current Injection as an Alternative Radiated Susceptibility Test Enforcing a Statistically Quantified Overtesting Margin. *IEEE Trans. Electromagn. Compat.* **2018**, *60*, 1270–1278. [CrossRef]

101. Cai, S.; Li, Y.; Zhu, H.; Wu, X.; Su, D. A Novel Electromagnetic Compatibility Evaluation Method for Receivers Working under Pulsed Signal Interference Environment. *Appl. Sci.* **2021**, *11*, 9454. [CrossRef]
102. Razek, A. Assessment of EMF Troubles of Biological and Instrumental Medical Questions and Analysis of Their Compliance with Standards. *Standards* **2023**, *3*, 227–239. [CrossRef]
103. Chen, C.H.; Huang, C.Y.; Huang, Y.C. Improving the electromagnetic compatibility of electronic products by using response surface methodology and artificial neural network. *Microelectron. Int.* **2022**, *39*, 1–13. [CrossRef]
104. Yang, Y.; Zeng, S.; Li, X.; Hu, Z.; Zheng, J. Ultrahigh and Tunable Electromagnetic Interference Shielding Performance of PVDF Composite Induced by Nano-Micro Cellular Structure. *Polymers* **2022**, *14*, 234. [CrossRef] [PubMed]
105. Wang, G.; Wang, L.; Mark, L.H.; Shaayegan, V.; Wang, G.; Li, H.; Zhao, G.; Park, C.B. Ultralow-Threshold and Lightweight Biodegradable Porous PLA/MWCNT with Segregated Conductive Networks for High-Performance Thermal Insulation and Electromagnetic Interference Shielding Applications. *ACS Appl. Mater. Interfaces* **2018**, *10*, 1195–1203. [CrossRef] [PubMed]
106. Yao, B.; Hong, W.; Chen, T.; Han, Z.; Xu, X.; Hu, R.; Hao, J.; Li, C.; Li, H.; Perini, S.E.; et al. Highly Stretchable Polymer Composite with Strain-Enhanced Electromagnetic Interference Shielding Effectiveness. *Adv. Mater.* **2020**, *32*, e1907499. [CrossRef]
107. Yun, T.; Kim, H.; Iqbal, A.; Cho, Y.S.; Lee, G.S.; Kim, M.; Kim, S.J.; Kim, D.; Gogotsi, Y.; Kim, S.O.; et al. Electromagnetic Shielding of Monolayer MXene Assemblies. *Adv. Mater.* **2020**, *32*, e1906769. [CrossRef] [PubMed]
108. Song, W.L.; Cao, M.S.; Lu, M.M.; Bi, S.; Wang, C.Y.; Liu, J.; Yuan, J.; Fan, L.Z. Flexible graphene/polymer composite films in sandwich structures for effective electromagnetic interference shielding. *Carbon* **2014**, *66*, 67–76. [CrossRef]
109. Song, W.L.; Guan, X.T.; Fan, L.Z.; Cao, W.Q.; Wang, C.Y.; Cao, M.S. Tuning three-dimensional textures with graphene aerogels for ultra-light flexible graphene/texture composites of effective electromagnetic shielding. *Carbon* **2015**, *93*, 151–160. [CrossRef]
110. Tan, Y.J.; Li, J.; Gao, Y.; Li, J.; Guo, S.; Wang, M. A facile approach to fabricating silver-coated cotton fiber non-woven fabrics for ultrahigh electromagnetic interference shielding. *Appl. Surf. Sci.* **2018**, *458*, 236–244. [CrossRef]
111. Han, M.; Yin, X.; Hantanasirisakul, K.; Li, X.; Iqbal, A.; Hatter, C.B.; Anasori, B.; Koo, C.M.; Torita, T.; Soda, Y.; et al. Anisotropic MXene aerogels with a mechanically tunable ratio of electromagnetic wave reflection to absorption. *Adv. Opt. Mater.* **2019**, *7*, 1900267. [CrossRef]
112. Cheng, J.; Li, C.; Xiong, Y.; Zhang, H.; Raza, H.; Ullah, S.; Wu, J.; Zheng, G.; Cao, Q.; Zhang, D.; et al. Recent Advances in Design Strategies and Multifunctionality of Flexible Electromagnetic Interference Shielding Materials. *Nano-Micro Lett.* **2022**, *14*, 80. [CrossRef]
113. Mohammad, M.; Wodajo, E.T.; Choi, S.; Elbuluk, M.E. Modeling and Design of Passive Shield to Limit EMF Emission and to Minimize Shield Loss in Unipolar Wireless Charging System for EV. *IEEE Trans. Power Electron.* **2019**, *34*, 12235–12245. [CrossRef]
114. Canova, A.; Corti, F.; Laudani, A.; Lozito, G.M.; Quercio, M. Innovative shielding technique for wireless power transfer systems. *IET Power Electron.* **2023**, *2023*, 1–8. [CrossRef]
115. Maxwell, J.C., VIII. A dynamical theory of the electromagnetic field. *Philos. Trans. R. Soc.* **1865**, *155*, 459–512. [CrossRef]
116. Nunes, A.S.; Dular, P.; Chadebec, O.; Kuo-Peng, P. Subproblems Applied to a 3-D Magnetostatic Facet FEM Formulation. *IEEE Trans. Magn.* **2018**, *54*, 7402209. [CrossRef]
117. Batra, T.; Schaltz, E.; Ahn, S. Effect of ferrite addition above the base ferrite on the coupling factor of wireless power transfer for vehicle applications. *J. Appl. Phys.* **2015**, *117*, 17D517. [CrossRef]
118. Piriou, F.; Razek, A. Numerical simulation of a nonconventional alternator connected to a rectifier. *IEEE Trans. Energy Convers.* **1990**, *5*, 512–518. [CrossRef]
119. Padilha, J.B.; Kuo-Peng, P.; Sadowski, N.; Batistela, N.J. Vector Hysteresis Model Associated to FEM in a Hysteresis Motor 691 Modeling. *IEEE Trans. Magn.* **2017**, *53*, 7402004. [CrossRef]
120. Ren, Z.; Razek, A. A coupled electromagnetic-mechanical model for thin conductive plate deflection analysis. *IEEE Trans. Magn.* **1990**, *26*, 1650–1652. [CrossRef]
121. Hariri, H.; Bernard, Y.; Razek, A. 2-D Traveling Wave Driven Piezoelectric Plate Robot for Planar Motion. *IEEE/ASME Trans. Mechatron.* **2018**, *23*, 242–251. [CrossRef]
122. Li, C.; Ren, Z.; Razek, A. An approach to adaptive mesh refinement for three-dimensional eddy-current computations. *IEEE Trans. Magn.* **1994**, *30*, 113–117. [CrossRef]
123. Gabriel, C.; Gabriel, S.; Corthout, E. The Dielectric Properties of Biological Tissues: II. Measurements in the Frequency Range 10 Hz to 20 GHz. *Phys. Med. Biol.* **1996**, *41*, 2251–2269. [CrossRef] [PubMed]
124. Barchanski, A.; Steiner, T.; De Gersem, H.; Clemens, M.; Weiland, T. Local Grid Refinement for low-Frequency Current Computations in 3-D Human Anatomy Models. *IEEE Trans. Magn.* **2006**, *42*, 1371–1374. [CrossRef]
125. Hasgall, P.; Neufeld, E.; Gosselin, M.C.; Kingenböck, A.; Kuster, N. IT'IS Database for Thermal and Electromagnetic Parameters of Biological Tissues. 2012. Available online: https://itis.swiss/virtual-population/tissue-properties/overview/ (accessed on 1 November 2023).
126. Makarov, S.N.; Noetscher, G.M.; Yanamadala, J.; Piazza, M.W.; Louie, S.; Prokop, A.; Nazarian, A.; Nummenmaa, A. Virtual Human Models for Electromagnetic Studies and Their Applications. *IEEE Rev. Biomed. Eng.* **2017**, *10*, 95–121. [CrossRef] [PubMed]
127. Noetscher, G.M. The CAD-Compatible VHP-Male Computational Phantom. In *Brain and Human Body Modeling 2020: Computational Human Models Presented at EMBC 2019 and the BRAIN Initiative® 2019 Meeting*; Makarov, S.N., Noetscher, G.M., Nummenmaa, A., Eds.; Springer: Cham, Switzerland, 2020; pp. 309–323. [CrossRef]

128. Ma, Z.; Deng, Z.; Zhou, X.; Li, L.; Jiao, C.; Ma, H.; Yu, Z.Z.; Zhang, H.B. Multifunctional and magnetic MXene composite aerogels for electromagnetic interference shielding with low reflectivity. *Carbon* **2023**, *213*, 118260. [CrossRef]
129. Yun, J.; Zhou, C.; Guo, B.; Wang, F.; Zhou, Y.; Ma, Z.; Qin, J. Mechanically strong and multifunctional nano-nickel aerogels based epoxy composites for ultra-high electromagnetic interference shielding and thermal management. *J. Mater. Res. Technol.* **2023**, *24*, 9644–9656. [CrossRef]
130. Verma, R.; Thakur, P.; Chauhan, A.; Jasrotia, R.; Thakur, A. A review on MXene and its' composites for electromagnetic interference (EMI) shielding applications. *Carbon* **2023**, *208*, 170–190. [CrossRef]
131. Razek, A. Thermal effects of electromagnetic origin from heating processes to biological disturbances due to field exposure—A review. *Therm. Sci. Eng.* **2023**, *6*, 20–33. [CrossRef]